Introduction to Making a Magnetogram Dr. K. D. Leka
July 26, 2023

Pre-Lecture Questions:

1: (This is a little bit of an English-language question): Can we measure the magnetic fields on the Sun?
2: Where (on the Sun) are the magnetic fields reported in (*e.g.*) HMI magnetograms from?
3: If the line-of-sight component is: B_ℓ or $\mathrm{B}_{\parallel} = 100 \pm 20$ and the component transverse to the line-of-sight is B_t or $\mathrm{B}_{\perp} = 100 \pm 20$, what is the *radial* component (B_r) of the field, and its uncertainty?

Note: none of the topics listed will be treated in-depth; references are provided and interested people are encouraged to see those and ask me about additional resources. I assume an undergraduate-level understanding of relevant physics.

Contents

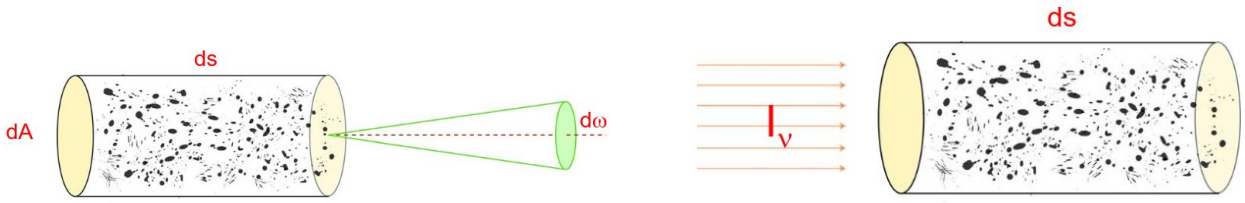

Figure 1: Visualization cartoon of emission (left) and absorption (right); from Konstantin Dellyanis' Stellar Atmospheres course notes, U. Hawai'i.

1 Radiative Transfer and Spectroscopy

With light traveling through a plasma, the interactions between the plasma and the photon(s) become very important. Key concepts:

Intensity and Radiation: *Specific Intensity:* constant energy transfer by light along rays. With no absorption or emission, this is conserved. *Radiative Flux:* the intensity through a surface at a specific wavelength. Integrated over 4π and all wavelengths, one obtains the "total intensity flux". *Absorption:* amount of intensity removed along a path $\mathrm{d}s$, $\kappa_\nu = n\,\sigma_\nu$ is the absorption (cm^{-1}) with frequency, over $\mathrm{d}s$ length of plasma. *Emission:* amount of intensity (energy) added within a volume of plasma ($\mathrm{d}V = \mathrm{d}A\,\mathrm{d}s$) into (along a path) of a solid angle (into a cone of size) $\mathrm{d}\omega$ wide. A unit of emission is $\mathrm{d}E_\nu^{\mathrm{emission}} = \epsilon_\nu\,\mathrm{d}V\,\mathrm{d}\omega\,\mathrm{d}\nu\,\mathrm{d}\tau$, where ϵ_ν is the emission coefficient (erg cm^{-3} sr^{-1} Hz^{-1} s^{-1}).

Optical Depth & Mean Free Path:

$$\begin{aligned} dI_\nu &= -\kappa_\nu I_\nu \mathrm{d}s \\ I_\nu(s) &= I_\nu^0 e^{-\int_0^s \kappa_\nu \mathrm{d}s} \\ \tau_\nu &= \int_0^S \kappa_\nu \mathrm{d}s \\ &\text{or} \\ \mathrm{d}\tau_\nu &= \kappa_\nu \mathrm{d}s \qquad (1) \\ &\text{also} \\ \tau_c &\equiv \int_S^{[obs,\ or\ \infty]} \chi_c \mathrm{d}s, \qquad (2) \end{aligned}$$

τ_c is the optical depth in the continuum, with $\tau_c = 0$ being the end point of the photon propagation or the observer (increases against propagation), and χ_{cont} is the continuum absorption. When $\tau_\nu = 1$, that means the photons have a mean free path of s before getting absorbed again. With only absorption:

$$\begin{aligned} I_\nu(s) &= I_\nu^0\, e^{-\tau} \qquad (3) \\ &\text{with} \\ \tau_\nu = 1 &\rightarrow I_\nu = I_\nu^0/e \\ &\simeq 0.37 I_\nu^0 \qquad (4) \end{aligned}$$

Optical Thickness indicates (1) the fraction of intensity passing through a layer, (2) how far "through" an atmosphere we can see. *Remember! this is all as a function of ν, or wavelength.*

Combine absorption with emission:

$$\mathrm{d}I_\nu/\mathrm{d}s = -\kappa_\nu I_\nu + \epsilon_\nu \qquad (5)$$

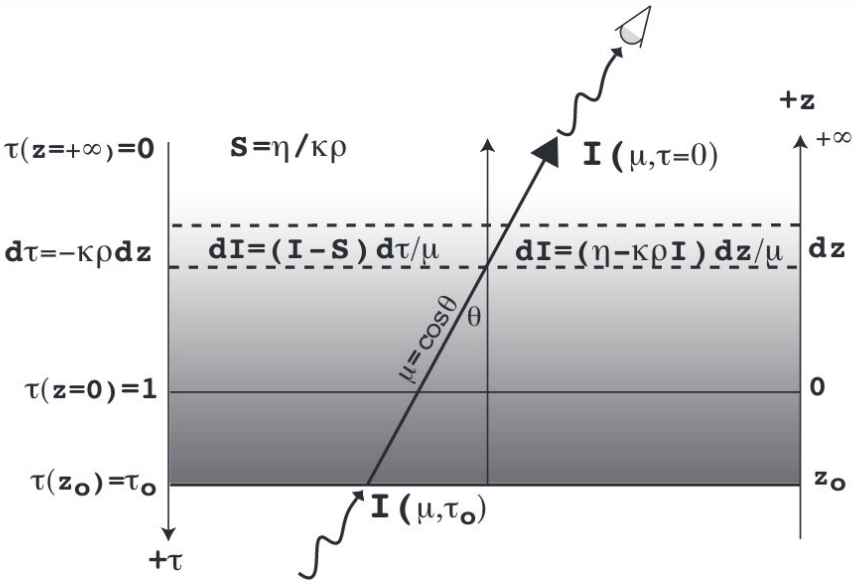

Fig. 5.— Illustration of the emergent intensity from emission and absorption in a stratified planar atmosphere. The lower boundary at $z = z_o$ and $\tau = \tau_o$ is assumed to have an intensity $I(\mu, \tau_o)$, where $\mu = \cos\theta$ is the vertical projection cosine of the ray.

Figure 2: Figure 5 from Stan Owocki's RT notes.

---

which is the "Radiative Transfer Equation": how much intensity per unit travel-length is removed and how much is added. Again Remember! as a function of frequency.

Line Formation: Consider the above *with* angle of ray different from gravity (θ, $\mu = \cos(\theta)$, *with* emission and absorption:

$$\mu \frac{\mathrm{d}I_\nu(\mu_\nu, \tau_\nu)}{\mathrm{d}\tau_\nu} = I_\nu(\mu_\nu, \tau_\nu) - S_\nu(\mu_\nu, \tau_\nu) \tag{6}$$

where $S_\nu = \epsilon_\nu/\kappa_\nu$.

The physics is in the two terms I_ν and S_ν. In integral form, for upward-propagating rays (toward smaller optical depth):

$$I(\mu, \tau) = I(\mu, \tau_0)e^{(\tau - \tau 0)/\mu} + \int_\tau^{\tau_0} S(\tau')e^{(-\tau' + \tau)/mu} d\tau'/\mu; \mu > 0, \tau < \tau_0 \tag{7}$$

while for downward-propagating (toward larger optical depth) rays:

$$I(\mu, \tau) = \int_\tau^{\tau_0} S(\tau')e^{(-\tau' + \tau)/|mu|} d\tau'/\mu; \mu < 0, \tau < \tau_0 \tag{8}$$

assuming no radiation is illuminating from the "top" (smaller τ) (e.g. $I(\mu, \tau = 0) = 0$.

Consider a simple case, the emergent intensity seen by a far-away observer ($\tau = 0$) from a "slab" of material (Figure 2):

$$I(\mu, 0) = \int_0^{\infty} S(\tau')e^{(-\tau')/mu} d\tau'/\mu; \mu > 0 \tag{9}$$

If we consider the source function to be linear (only changing with respect to) optical depth, $S(\tau') = a + b\tau'$ then integrating by parts one gets:

$$I(\mu, 0) = a + b\mu = S(\tau = \mu) \tag{10}$$

which, if one uses "≈" instead of =, is the Eddington-Barbier (EB) relation. This is a "first order" explanation for limb-darkening in the Sun: at disk-center, $\mu = 1$ and it is the local "planar" atmosphere. Away from disk-center, and assuming local thermodynamic equilibrium (LTE, so brightness is a function of temperature), the E-B relation provides the brightness ratio that you can expect:

$$\frac{I(\mu \to 0, 0)}{I(1, 0)} = \frac{a + b\mu}{a + b} = \frac{S(\tau = 0)}{S(\tau = 0) + dS/d\tau} \approx \frac{B(\tau = 0)}{B(\tau = 0) + dB/d\tau}. \tag{11}$$

Brightness increases with increasing Temperature, and a stellar atmosphere (generally) gets cooler with height, so $dB/d\tau > 0$, and $I(\mu \to 0, 0)/I(1, 0) < 1$ or the emergent intensity decreases with increasing μ.

Now returning to the ν situation: optical depth earlier was related to the mean-free-path of a photon. We can look at the probability of a photon being absorbed ($e^{-\tau_\nu} d\tau_\nu$) as related to optical depth:

$$\langle \tau_\nu \rangle = \int_0^\infty \tau_\nu e^{-\tau_\nu} d\tau_\nu = 1 \tag{12}$$

means that, if you have constant absorption coefficients ($\kappa_\nu(s) = \text{constant}$) then $\Delta\tau_\nu = \kappa_\nu(s)\Delta s$ which implies that $\bar{s} = 1/\kappa_\nu(s)$.

The probability of a photon being absorbed, however, is very much a function of ν. When ν is the same as the excitation frequency for a spectral line (level transition), $\kappa_\nu(s)$ increases: there is a high probability of that photon being absorbed, the mean free path decreases. When ν corresponds to "continuum", away from atomic (or molecular) transition frequencies, $\kappa_\nu(s)$ decreases.

So, the "$\tau = 1$" layer where optical depth is unity (where we can "see to" in an atmosphere) is higher when $\kappa_\nu(s)$ is larger (less density is required for the same absorption probability), such as at a "line-center" wavelength, than in the continuum (and we thus see "deeper" in to the atmosphere). If the source function is greater than the absorption, then we get emission lines (Figure 3).

Spectral Line Shape and Curves of Growth: The frequency ν of an atomic transition has a natural range according to the probability of transition. The absorption coefficient at that energy/frequency is simply:

$$\kappa = \int_0^\infty \frac{h\nu}{4\pi}(n_1 B_{12} - n_2 B_{21}) \tag{13}$$

that is, a function of the Planck constant, frequency, level populations (n) and the transition's Enstein coefficients, which are effectively a probability of absorption / emission. *This is not a $\delta-$function, but is extremely narrow.*

A short list of factors that influence observed spectra line shapes (assuming a homogeneous plasma):

• Temperature: Increased plasma temperature produces Doppler shifts, change the frequency at which the absorption is most likely; generaly symmetric about ν_0. Related: microturbulence.

• Density: as this increases, spectral lines get deeper (stronger) and the "wings" get broader and change shape. Related: damping. See Figure4.

• Velocity: the bulk velocity of the plasma shifts the absorption peak relative to ν_0 but otherwise would not change the line shape.

• Spectral Blends: other spectral lines very nearby.

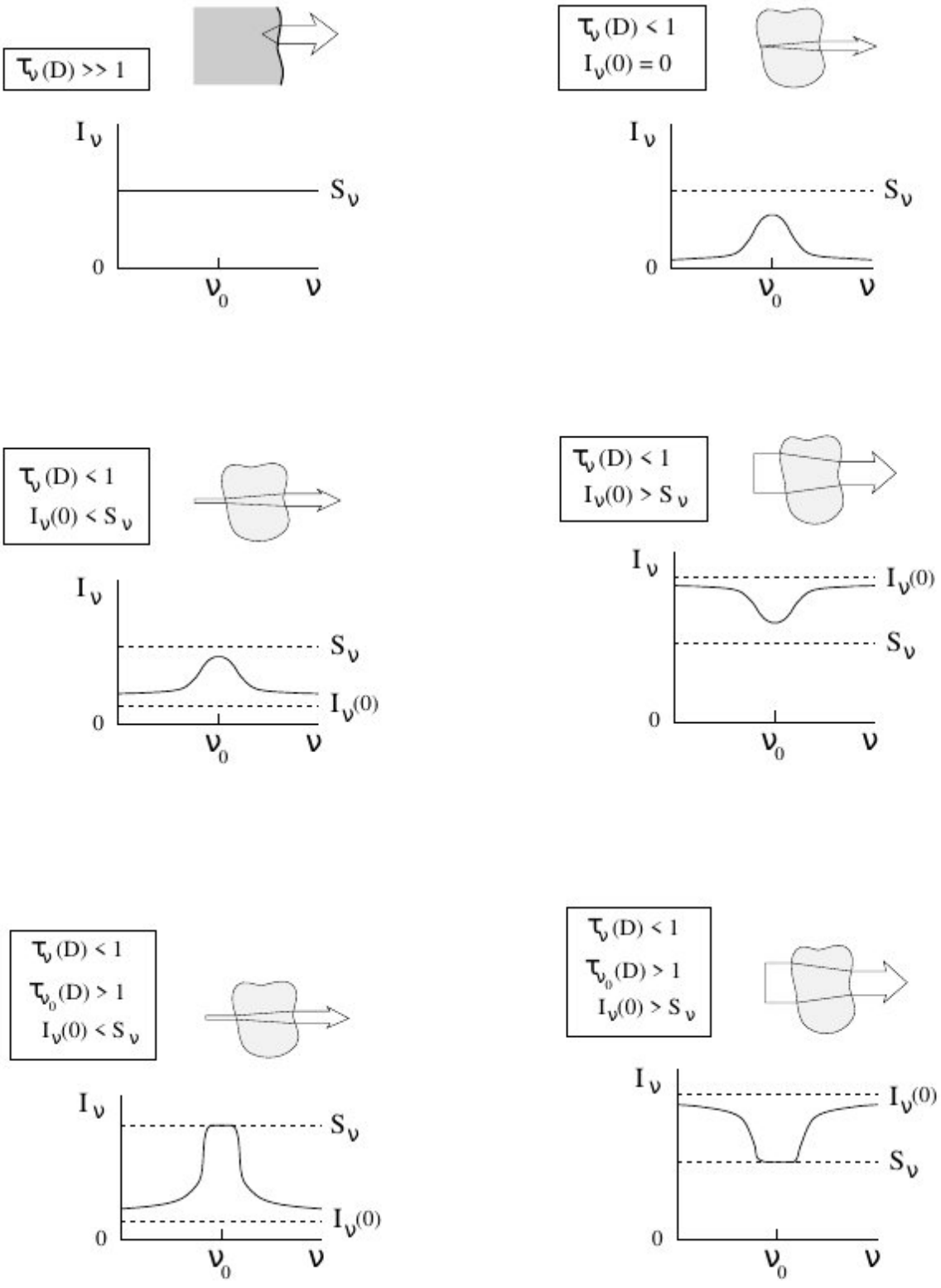

Figure 2.2: Spectral lines from a homogeneous object with $S_\nu^l = S_\nu^c = S_\nu$ everywhere, according to (2.35)–(2.36). No lines emerge when the object is optically thick (top left). When it is optically thin, emission lines emerge when the object is not back-lit ($I_\nu(0) = 0$, top right), or when it is illuminated with $I_\nu(0) < S_\nu$. Absorption lines emerge only when the object is optically thin and $I_\nu(0) > S_\nu$. The emergent lines saturate to $I_\nu \approx S_\nu$ when the object is optically thick at line center.

Figure 3: Emission, Absorption, optical thickness. From [17].

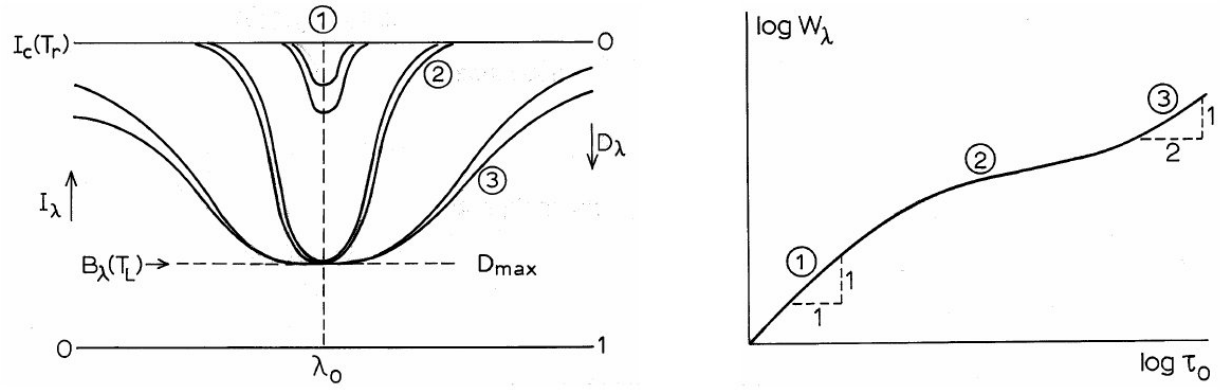

Figure 9.1: Line profiles and curve of growth in the Schuster-Schwarzschild model. Weak lines have Gaussian shapes. Their area grows linearly with the amount of extinction. The curve of growth flattens when lines become saturated because the reversing layer becomes optically thick at line center. The curve of growth rises again when optically thin damping wings develop. This plot is for absorption lines with $T_L < T_R$. From Zwaan (1993).

Figure 4: From [17].

• The Thermodynamic environment: LTE? NLTE? Scattering?

• The Radiation environment: sources of irradiance (source function) that are not local.

• The ElectroMagnetic environment: electric fields, and magnetic fields.

The above changes dramatically if *e.g.* $T(\tau), \rho(\tau), V_{\rm Dopp}(\tau)$! Then asymmetries can be introduced.

Take-Away Points:

• Plasma properties define the optical depth scale. The $\tau_\nu = 1$ "surface" depends on the local plasma density, temperature, composition, ionization, *etc.*

• Spectral lines provide information on the plasma properties by their shapes and behavior. But the same shape/behavior can be produced by different properties.

• The $\tau_\nu = 1$ surface is deeper in continuum wavelengths, higher (at lower density) at the line-center where absorption (emission) is more probable.

Relevant Sources: [15], [also see all the references and links etc. in 17, which is best accessed through the associated website `https://robrutten.nl/rrweb/rjr-pubs/2021LingAstRep...2R.pdf`]; see other RT course notes: `https://www.bartol.udel.edu/~owocki/phys333/Phys633-notes1.pdf`.

2 Polarized Radiation and the Stokes Parameters

When a magnetic field is present, the energy levels for atomic transitions split (Zeeman splitting) and photons can become polarized. In solar physics the polarization states are described using Stokes formalism:

$$\mathbf{I} \equiv (I,\ Q,\ U,\ V)^T \tag{14}$$

where I represents unpolarized light, V is the circularly polarized component and Q, U are the linearly polarized components (oriented 45° apart, see Figure 5). The spectroscopy of polarized light is *spectropolarimetry*, and provides the *only direct information we have* on the

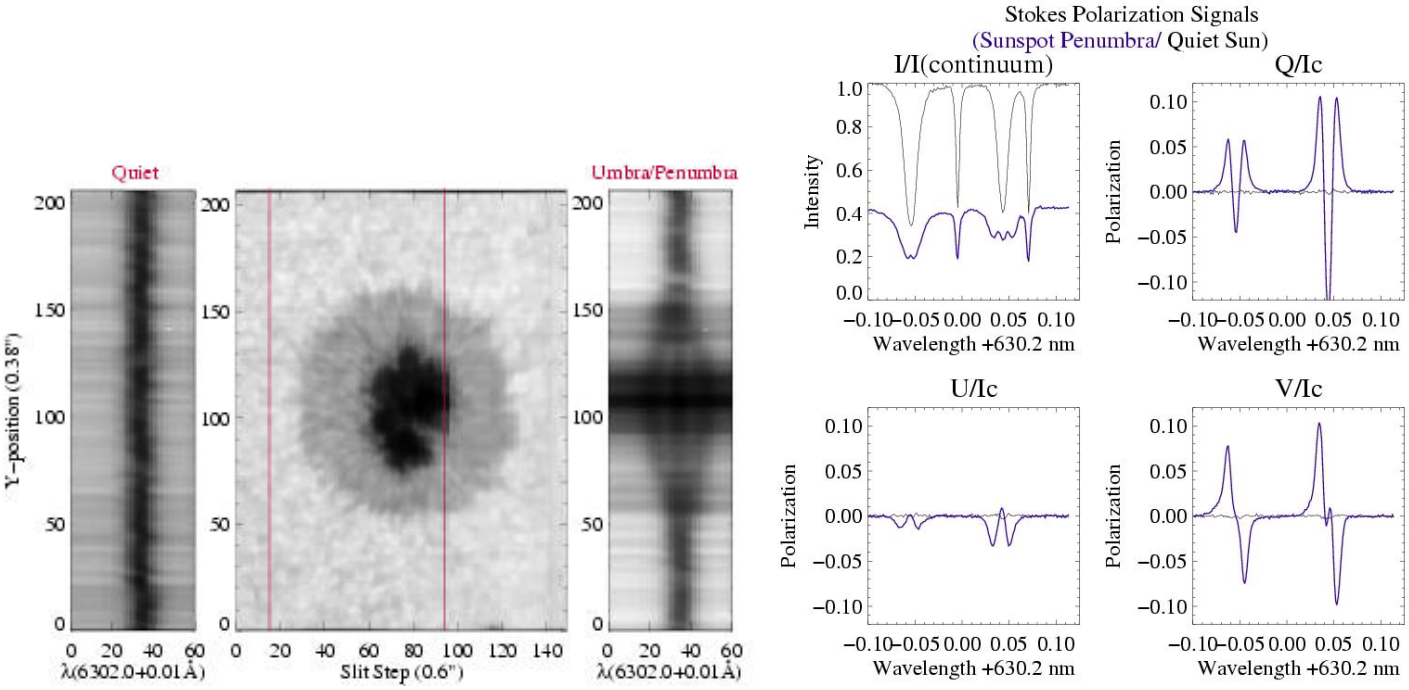

Figure 5: Left: sunspot and example spectra in a magnetically-sensitive line. Right: Spectra from a "quiet" area (black) and a sunspot umbra (blue), showing the Stokes polarization spectra.

---

solar magnetic fields. The degree or fraction of polarization $P = \sqrt{V^2 + U^2 + Q^2}/I$ and the degree of splitting are *generally* functions of field strength *for resolved structures:*

$$\Delta\lambda_Z \propto g_L \, \lambda^2 \, |B| \tag{15}$$

with g_L being the Landé factor for the transitions in question. In the Stokes formalism, the "instrument" or "sky" components and their orientation angle in the plane-of-the-sky (ϕ) produce the polarization:

$$\begin{aligned} \mathrm{B}_{\parallel} &\Rightarrow V \\ \mathrm{B}_{\perp} &\Rightarrow \sqrt{Q^2 + U^2} \\ \phi &\Rightarrow \tan^{-1}(U/Q), \phi \in [0°, 180°]. \end{aligned} \tag{16}$$

However, going back to the RTE:

$$\mathrm{d}\mathbf{I}/\mathrm{d}\tau_c = \mathrm{K}(\mathbf{I} - \mathbf{S}) \tag{17}$$

now K is the "propagation matrix", **S** is the "source vector". In order to retrieve $\vec{B}$, we must account for the thermodynamics, radiation environment, plasma dynamics across the range of τ our chosen magnetically-sensitive ($g_L \neq 0$) samples. A full solution of the Radiative Transfer Equation *of Polarized Light* is required, but without simplifications, is not directly solvable because K is not fully known.

Take-Away Points:

• The polarization state *and* the line-splitting of a magnetically-sensitive spectral line have information on the magnetic field in the plasma.

• The Zeeman effect is *an additional* effect on spectral line-profile shapes and behavior.

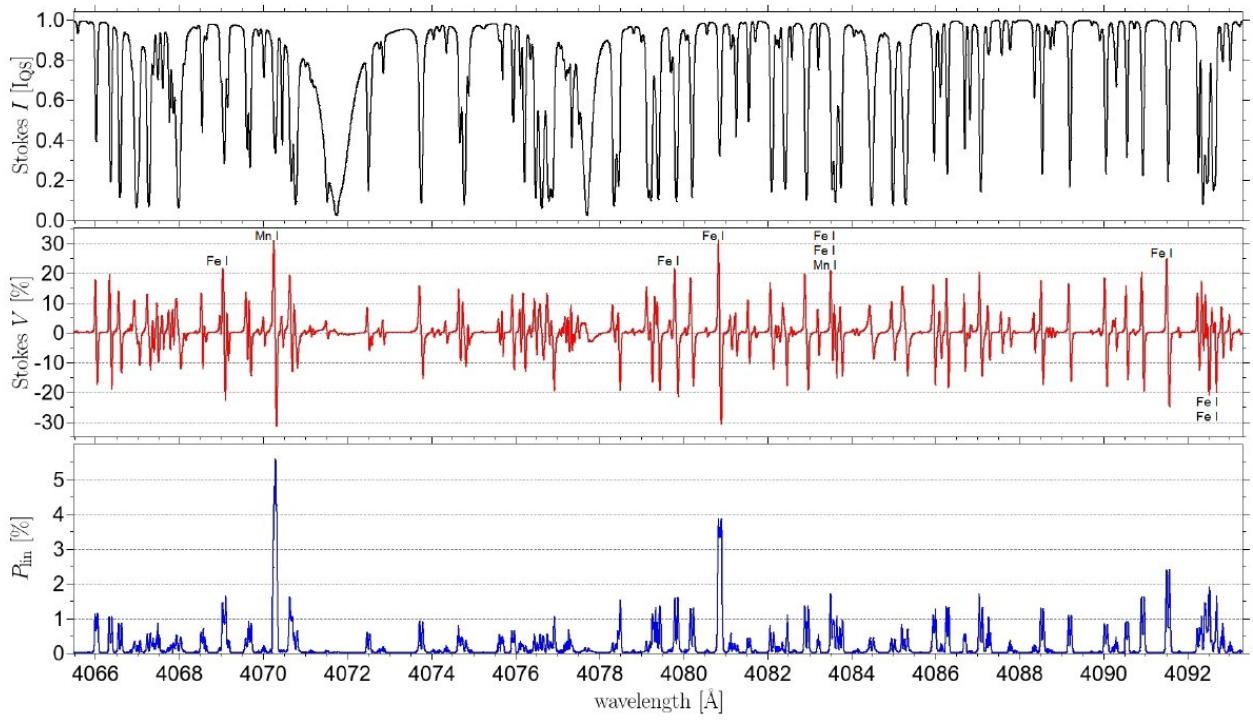

Figure 6: From Riethmuller & Solanki 2018, many solar absorption lines in the blue visible spectrum, and their circular polarization and polarization fraction. Note some strong lines are not magnetically sensitive and show no polarization, while some less-strong lines show high sensitivity to magnetic fields.

• Using the Stokes formalism:
magnetic field along the line-of-sight ∘ circular polarization ⇔ "V"
magnetic field perpendicular-to-line-of-sight ∘ linear polarization ⇔ "Q, U", with Q/U varying with orientation.

Relevant Sources: [21, 7, 2, 6]

3 Inversion Methods and Limitations

"Magnetograph Formula" for $B_{\parallel}$ only: $B_{\parallel} \propto V$. Saturates easily but there are sophisticated implementations (for MDI [18], and HMI [9]). *Advantages:* fast, *Disadvantages:* saturates, basic estimates, not vector.

"Weak Field Approximations" include "Derivative Methods" and "Integral methods". They use the almost-linear behavior of the polarization signals with $|B|$ in some [physical, wavelength] regimes ($\Delta\lambda_Z < \Delta\lambda_{\mathrm{D}opp}$, not-strong $|B|$) for more sophisticated estimates of the underlying fields:

$$\begin{aligned} B_{\parallel} &\propto \frac{V}{\mathrm{d}I/\mathrm{d}\lambda} \\ B_{\perp} &\propto \frac{\sqrt{Q^2+U^2}}{\mathrm{d}I^2/\mathrm{d}\lambda^2} \\ \phi &= \tan^{-1}(U/Q), \phi \in [0°, 180°]. \end{aligned} \tag{18}$$

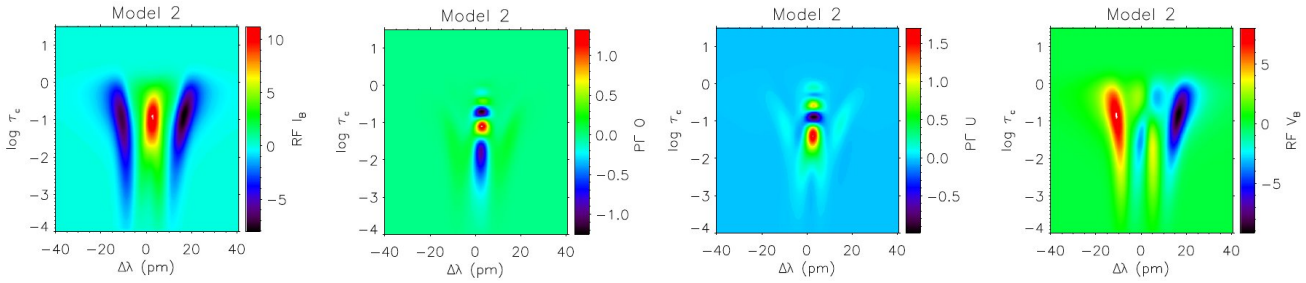

Figure 7: Response functions for (l:r) Stokes $[I,\ Q,\ U,\ V]$ for Field Strength $|\boldsymbol{B}|$ as a function of $\Delta\lambda$ from line center and $\log(\tau_c)$ the continuum optical depth, for a particular model atmosphere. Horizontal line for reference, shows the different responses as a $f(\tau)$. From del Torienesta & Ruiz Cobo 2016

The "integral method" uses the integral of the signals over the spectral line [16], whereas the "derivative methods" [11, 10, 4] generally evaluates the signals at a location in the line wings (not the core). *Advantages:* fast. *Disadvantages:* difficulties with unresolved structures, sensitive to Faraday rotation ("magneto-optical effects" caused when a plane-polarized wave travels through an ionized medium) that can create "fake" twist in $B_\perp$.

"Milne-Eddington Approximation" Inversions This is the most widely used for Zeeman-split photospheric data, in part because it can be solved analytically. Assumes LTE and a linear source function $S_\nu = S_0 + S_1\tau$. Assumes $\boldsymbol{B}, V_{Dopp}, P, \rho, T$ are *all* constant as $f(\tau)$. In other words, over the formation height range of the line in question:

$$\frac{\Upsilon_{\tau max} - \Upsilon_{\tau min}}{\Upsilon_{\tau max} + \Upsilon_{\tau min}} \ll 1 \ \forall\ \Upsilon \tag{19}$$

$\Upsilon \in$[density, temperature, pressure magnetic field strength & direction, plasma velcoity, ionization fraction]. Magneto-optical effects can be handled. ME-based inversions thus return an *average* inferred atmosphere over τ. (There is debate as to whether the thermodynamic parameters can be "believed" or not.) Additionally there are *many many* ways to implement a "ME-based inversion", and *these can lead to significantly different results!!* There is no one "ME inversion method". *Advantages:* returns good, average, representations; modern-day: reasonably fast. *Disadvantages:* sensitive to implementation and minimization algorithms; unpredictable failures when spectra are not consistent with ME assumptions.

"Response Function" analysis asks "how does the spectropolarimetric signal behave as $f[\boldsymbol{B},\ \rho,\ T,\ v_{Dopp},\ \tau]$. Through radiative transfer modeling, atmospheres are described in terms of $\partial X/\partial\tau$ where X is the plasma parameter. Figures 7, 8. *Advantages:* significant physics, retrieves τ-based gradients. *Disadvantages:* slow (this is improving), sensitive to implementation.

General approach: (1) Use something like the WFA to "start", then (2) use a global optimization method to find the atmosphere & $\boldsymbol{B}$ which produces the best fit between the forward-model emergent Stokes spectra and the observed spectra. Even still with sophisticated inversions, things fail (see, *e.g.*, [9] for examples with HMI, and see Figure 9 for an example with a more sophisticated inversion).

Take-Away Points:

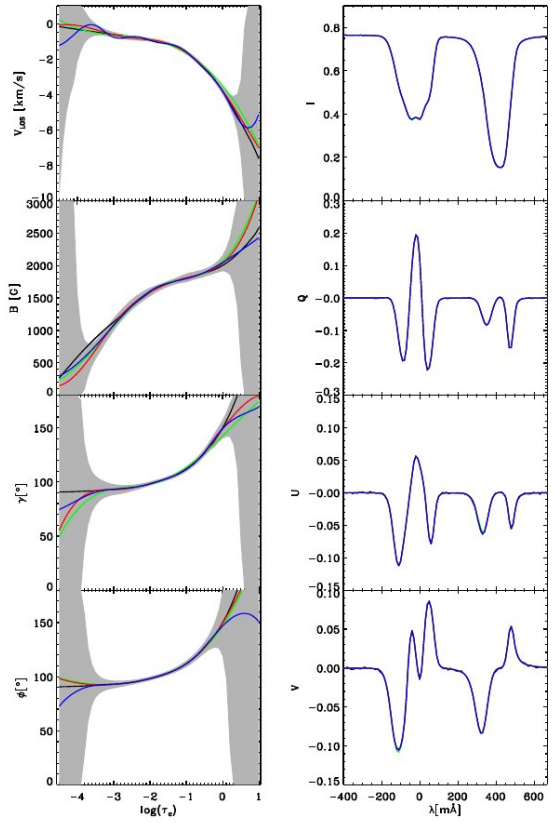

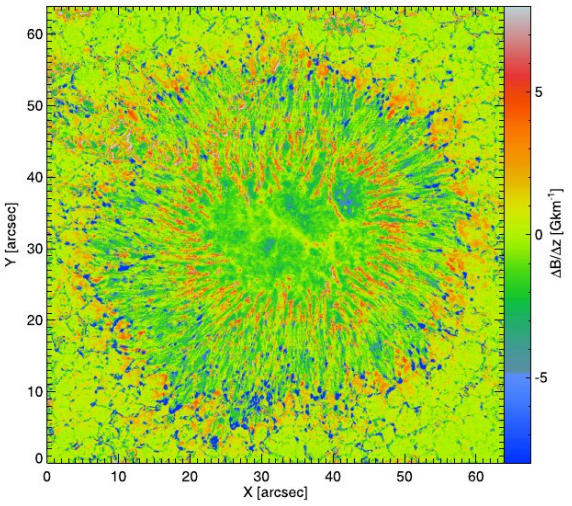

Figure 2 Gradient of the magnetic field computed between the geometrical height corresponding to the deepest nodes ($\log\tau = -0.9, 0$). A positive field gradient represents field strength increasing with height. Credit: Tiwari *et al.* (2015), reproduced with permission ©ESO.

Figure 8: Line profiles (midddle) and their fits using the Stokes Inversions based on Response Functions (SIR) code; residuals are $\ll 0.005$. The model atmospheres producing these fits (left) show the gradients in the plasma parameters. When applied to a full sunspot (right), one can obtain an estimate of (for example) field-strength gradients with height.

• Estimates of photospheric $\boldsymbol{B}$ can be made with different levels of simplification (assumptions) for the radiative transfer. *However*, the bigger the simplification, the larger the simplification of the result.

• Inversions produce $B_\parallel$, $B_\perp$, ϕ components of $\boldsymbol{B}$ in the "instrument / sky" frame of reference. *Remember:* the Sun is a sphere.

• Most "pipeline" photospheric magnetograms represent an *average* over the pixel area and height (τ or z).

Relevant sources: [3, 6, 12, 11]

4 Disambiguation and the "Image" *vs.* "Helio / Physical" Reference Frames

What is returned from inversions is not yet useful, it is only the components in the "image" plane, or "as the detector / telescope sees it", and the direction of $B_\perp$ is ambiguous to 180° due to a degeneracy in the level-splitting. To obtain *physically meaningful* components requires two steps: (1) determing the direction of $B_\perp$, (2) applying a coordinate transform such that $B_\parallel$, $B_\perp$, $\phi \Longrightarrow B_x$, B_y, B_z or $\Longrightarrow B_r$, B_ϕ, B_θ (Figures 10, 11). Note: the coordinate transform applies to the *vector components*; and is different from interpolating the data onto a different sampling grid.

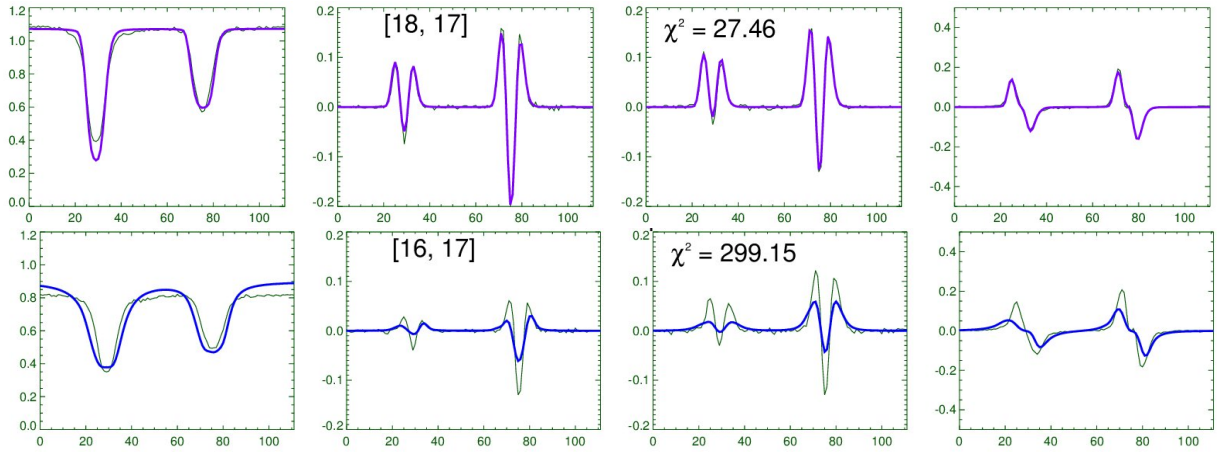

Figure 9: Even with sophisticated inversion and "fairly normal" (Milne-Eddington-like, with symmetric $[Q,\ U]$ and anti-symmetric $[V]$, sometimes the optimization failes to find a good fit between synthetic magnetized atmosphere and the data. Data (thin lines): from Hinode/SP. The two examples are very similar, only 2 pixels away from each other, and with very slight differences in the I profiles. Model fits (thick lines): from the NICOLE inversions [20]. Note the difference in χ^2.

The coordinate transform applies to all three components and returns all three components. Generally we take:

$$\begin{aligned} B_x^i &= \mathrm{B}_\perp \sin(\phi) \\ B_y^i &= \mathrm{B}_\perp \cos(\phi) \\ B_z^i &= \mathrm{B}_\parallel \end{aligned} \tag{20}$$

and then $\boldsymbol{B}^h = \mathbf{A}\boldsymbol{B}^i$, and $\mathbf{A}$ is a function of the location on the solar disk:

$$\mathbf{A} = \begin{pmatrix} axx & axy & axz \\ ayx & ayy & ayz \\ azx & azy & azz \end{pmatrix}$$

with these components depending on the solar p-angle, $b0$-angle, and the location of the target (latitude "bc" longitude "lc"):

$$\begin{aligned} axx &= -\sin(b0) * \sin(p) * \sin(lc) + \cos(p) * \cos(lc) \\ axy &= +\sin(b0) * \cos(p) * \sin(lc) + \sin(p) * \cos(lc) \\ axz &= -\cos(b0) * \sin(lc) \\ ayx &= -\sin(bc) * (\sin(b0) * \sin(p) * \cos(lc) + \cos(p) * \sin(lc)) - \cos(bc) * \cos(b0) * \sin(p) \\ ayy &= +\sin(bc) * (\sin(b0) * \cos(p) * \cos(lc) - \sin(p) * \sin(lc)) + \cos(bc) * \cos(b0) * \cos(p) \\ ayz &= -\cos(b0) * \sin(bc) * \cos(lc) + \sin(b0) * \cos(bc) \\ azx &= +\cos(bc) * (\sin(b0) * \sin(p) * \cos(lc) + \cos(p) * \sin(lc)) - \sin(bc) * \cos(b0) * \sin(p) \\ azy &= -\cos(bc) * (\sin(b0) * \cos(p) * \cos(lc) - \sin(p) * \sin(lc)) + \sin(bc) * \cos(b0) * \cos(p) \\ azz &= +\cos(bc) * \cos(b0) * \cos(lc) + \sin(bc) * \sin(b0) \end{aligned} \tag{21}$$

The application of the (physical) assumptions must be done using the *physically-relevant* components $\boldsymbol{B}^h$, whereas the 180° "flips" are done for the *observed* components. Some methods apply "local dot-product" approaches, *e.g.:* "which direction is closest to the potential field?".

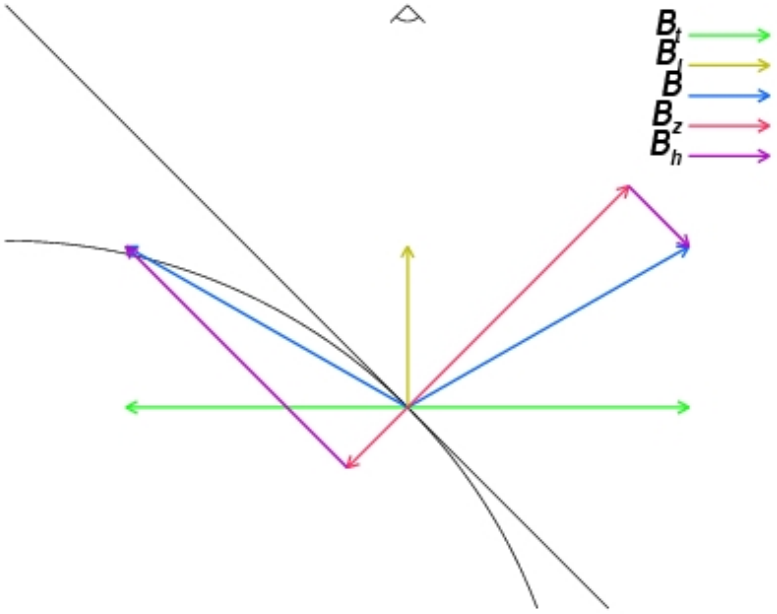

Figure 10: The two primary coordinate and component systems used for vector field reference: "image" or "instrument" or "plane of the sky" (yellow/green), or $B_\parallel, B_\perp, \phi$ and the "solar" or "heliographic" or "physical" (red / purple). The image-plane component perpendicular to the line-of-sight ($B_\perp$, green, two options) is ambiguous to 180°. The direction chosen for it, impacts what we believe is the "solar" vector (blue, two options).

Most well-performing methods use global optimization to minimize *e.g.:* total vertical current, angle between neighboring pixels, etc.

(See Movie)

Take-Away Points:

• What comes out of the inversions is *not yet useful*. The direction of $B_\perp$ must be selected.

• Changing $B_\perp$ by 180° does *not* change the heliographic or physical horizontal field by 180°; it influences all 3 physical components, according to field orientation and observing angle.

• All disambiguation algorithms make assumptions.

• "Garbage in, garbage out": if inversion fails, disambiguation cannot fix it.

Relevant sources: [8, 14, 9]

5 Instrumental Approaches

The Challenge: data are 4-D: $[x,\ y,\ \lambda,\ P]$ and generally detectors are 2-D. To make magnetic maps, science "use-cases" enter in; the lower priority dimensions are sampled slower, or less well. Examples:

Hinode/Spectropolarimeter science focus: high-accuracy Stokes spectra, high spatial resolution. Scanning-slit spectrograph provides $[y,\ \lambda,\ P]$ images, with a limited FOV; x-direction is the slow axis.

Helioseismic and Magnetic Imager science focus: vector data at a cadence to match good spatial resolution with photospheric motions, full disk. Imaging optics provide $[x,\ y]$ over full disk, with $[\lambda, P]$ slower, and limited samping.

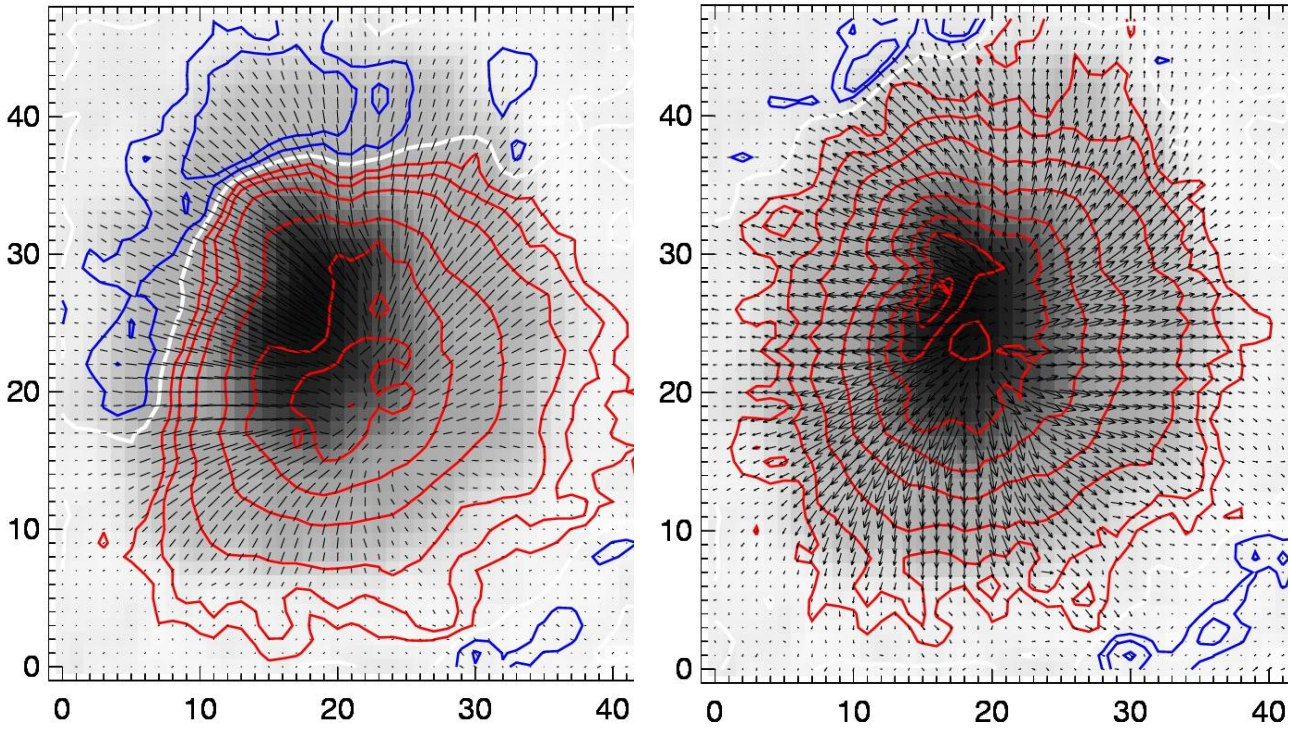

Figure 11: Left: Output from an inversion of a sunspot (N20 E20), Red/blue are $B_{\parallel}$ +ve/-ve, line *segments* indicate the strength & direction of $B_{\perp}$. Note the "apparent polarity inversion line". Right: after disambiguation, and after transforming to use the physical / local *components*, note the *arrows*, and the PIL has shifted to the edge of the sunspot. Note these are still plotted at the image *sampling*; the components have *not* been interpolated.

See Figure 12 for examples. What is desired is data that are well-sampled in time (cadence and longevity), and space (field-of-view, resolution). Multi-plexing collection (arrays of fibre-optic feeds) to simultaneously sample λ, P across an array imaging $[x, y]$, and are in development.

Also something to note: even with the 4 m DKIST telescope, high-resolution (in all dimensions) spectropolarimetry is *"photon-starved"*. It takes a lot of photons to detect signals with good signal-to-noise ratios.

Data Reduction has as its goal to remove all instrumental impacts so that the data are what the Sun produces. See [13, 19, 5] for examples of what it takes to develop the instrument-calibration matricies and covariances. [1] *Every* optical element *will* change the incoming photon. *Every* optical element including detectors have $< 100\%$ efficiency. *Every applied algorithm* includes assumptions that may be incorrect. The best input to (*e.g.*) the inversions are spectra *as they would be coming from the Sun*, which means correcting *each and every change* to the incoming light.

6 Sources of Uncertainty & Estimating Uncertainty

See "`HMI_error_analysis_intro.pdf`"

[1] Everyone who uses magnetograms should *briefly* look at these papers to appreciate the data reduction and calibration effort required to make a magnetogram!

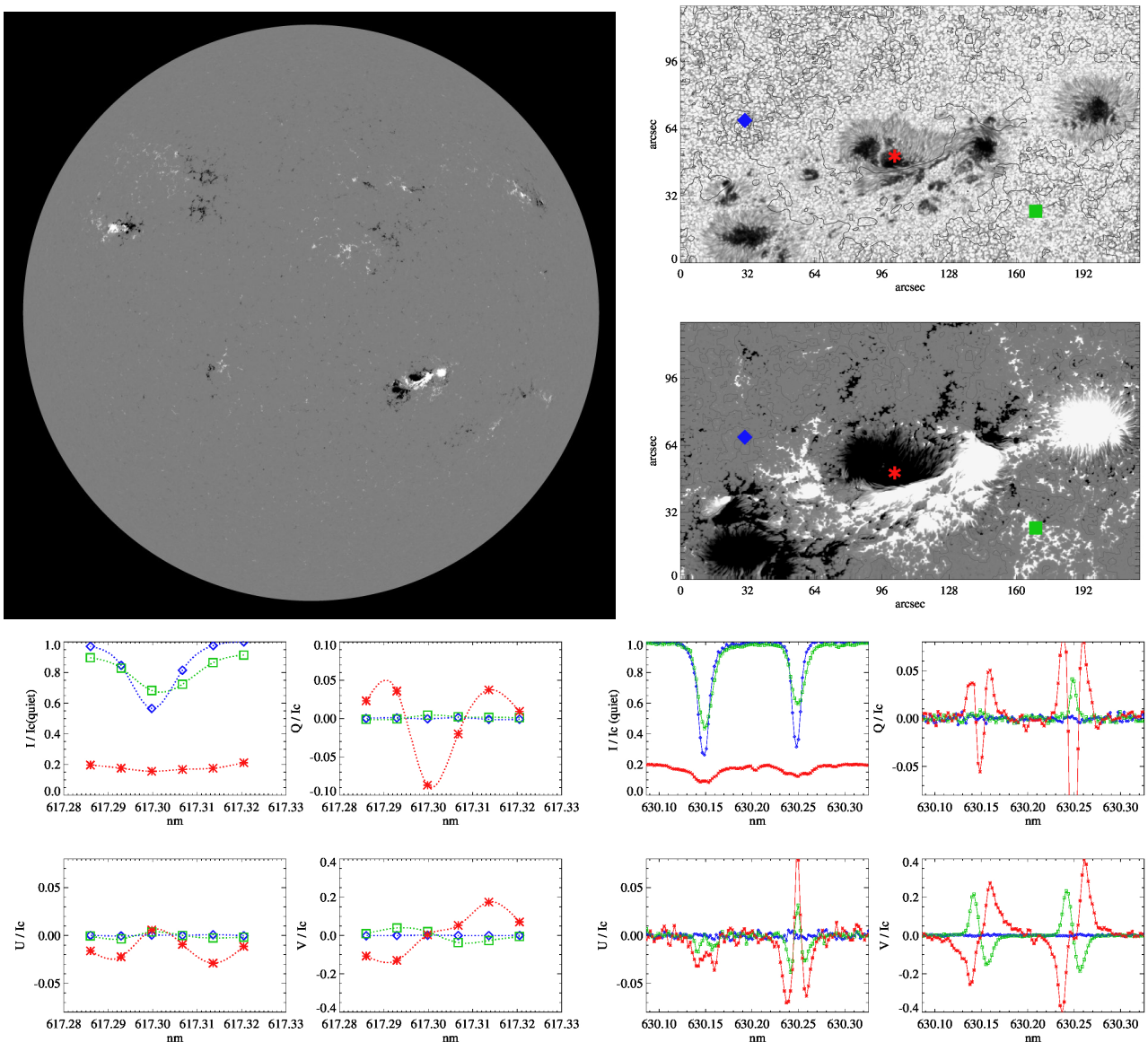

Figure 12: Top: Full-disk $B_{\|}$ image from HMI (left) and field-of-view images of continuum and $B_{\|}$ from Hinode/SP (right) of NOAA AR 11158 at 20110215_204800 TAI (south/west in full-disk image). Colored thick symbols in the right-hand images indicate (blue diamond) quiet Sun, (green square) nearby plage, (red star) umbral edge. Spectra are from HMI (left) and Hinode/SP (right), for the points indicated by color. Note for HMI spectra, the sampled points are connected artificially. HMI optimizes spatial "integrity" (the spatial relationships between features on the image are "true") and coverage (full disk), temporal cadence, and continuous coverage. Hinode/SP optimizes spectral accuracy and sampling and high spatial resolution. HMI thus sacrifices spectral sampling and resolution, and has moderate $1''$ spatial resolution; Hinode/SP thus sacrifies temporal cadence (an image can take 20-60min to "build" from slit-steps) and field-of-view, with target-specified spatial coverage. From [1].

7 Discussion of Introductory Questions

The following are some guides for your answers:
1: Focus on the word "measure" which implies "directly measure". Use an English Thesaurus to explore different words, remembering that "all we have are photons".

2: Question (for guidance): are the optical-depth scale τ and physical scale (in the $-1*$gravity direction z) the same?

3: Question (for guidance): do you have all the information you need?

References

[1] G. Barnes and K. D. Leka. Inferring Currents from the Zeeman Effect at the Solar Surface. In A. Keiling, O. Marghitu, and M. Wheatland, editors, *Electric Currents in Geospace and Beyond*, volume 235 of *Washington DC American Geophysical Union Geophysical Monograph Series*, pages 81–91, March 2018. doi: 10.1002/9781119324522.ch5.

[2] J. M. Borrero and K. Ichimoto. Magnetic Structure of Sunspots. *Living Reviews in Solar Physics*, 8:4, September 2011. doi: 10.12942/lrsp-2011-4.

[3] R. Centeno, J. Schou, K. Hayashi, A. Norton, J. T. Hoeksema, Y. Liu, K. D. Leka, and G. Barnes. The Helioseismic and Magnetic Imager (HMI) Vector Magnetic Field Pipeline: Optimization of the Spectral Line Inversion Code. *Sol. Phys.*, 289:3531–3547, September 2014. doi: 10.1007/s11207-014-0497-7.

[4] Rebecca Centeno. On the Weak Field Approximation for Ca 8542 Å. *apj*, 866(2):89, October 2018. doi: 10.3847/1538-4357/aae087.

[5] S. Couvidat, J. Schou, R. A. Shine, R. I. Bush, J. W. Miles, P. H. Scherrer, and R. L. Rairden. Wavelength Dependence of the Helioseismic and Magnetic Imager (HMI) Instrument onboard the Solar Dynamics Observatory (SDO). *Sol. Phys.*, 275:285–325, January 2012. doi: 10.1007/s11207-011-9723-8.

[6] J. C. del Toro Iniesta and B. Ruiz Cobo. Inversion of the radiative transfer equation for polarized light. *Living Reviews in Solar Physics*, 13:4, December 2016. doi: 10.1007/s41116-016-0005-2.

[7] Jose Carlos del Toro Iniesta. *Introduction to Spectropolarimetry*. Cambridge University Press, April 2003. ISBN 0521818273.

[8] G. A. Gary and M. J. Hagyard. Transformation of Vector Magnetograms and the Problems Associated with the Effects of Perspective and the Azimuthal Ambiguity. *Sol. Phys.*, 126: 21–36, 1990.

[9] J. T. Hoeksema, Y. Liu, K. Hayashi, X. Sun, J. Schou, S. Couvidat, A. Norton, M. Bobra, R. Centeno, K. D. Leka, G. Barnes, and M. Turmon. The Helioseismic and Magnetic Imager (HMI) Vector Magnetic Field Pipeline: Overview and Performance. *Sol. Phys.*, 289:3483–3530, September 2014. doi: 10.1007/s11207-014-0516-8.

[10] J. Jefferies and D. L. Mickey. On the Inference of Magnetic Field Vectors from Stokes Profiles. *ApJ*, 372:694–702, 1991.

[11] J. Jefferies, B. W. Lites, and A. Skumanich. Transfer of Line Radiation in a Magnetic Field. *ApJ*, 343:920–935, 1989.

[12] K. D. Leka, Eric L. Wagner, Ana Belén Griñón-Marín, Véronique Bommier, and Richard E. L. Higgins. On Identifying and Mitigating Bias in Inferred Measurements for Solar Vector Magnetic-Field Data. *solphys*, 297(9):121, September 2022. doi: 10.1007/s11207-022-02039-9.

[13] B. W. Lites, D. L. Akin, G. Card, T. Cruz, D. W. Duncan, C. G. Edwards, D. F. Elmore, C. Hoffmann, Y. Katsukawa, N. Katz, M. Kubo, K. Ichimoto, T. Shimizu, R. A. Shine, K. V. Streander, A. Suematsu, T. D. Tarbell, A. M. Title, and S. Tsuneta. The Hinode Spectro-Polarimeter. *Sol. Phys.*, 283:579–599, April 2013. doi: 10.1007/s11207-012-0206-3.

[14] T. R. Metcalf, K. D. Leka, G. Barnes, B. W. Lites, M. K. Georgoulis, A. A. Pevtsov, G. A. Gary, J. J ing, K. S. Balasubramaniam, J. Li, Y. Liu, H . N. Wang, V. Abramenko, V. Yurchyshyn, and Y.-J. Moon. An Overview of Existing Algorithms for Resolving the 180° Ambiguity in Vector Magnetic Fields: Quantitative Tests with Synthetic Data. *Sol. Phys.*, 237:267–296, 2006. doi: 10.1007/s11207-006-0170-x.

[15] D. Mihalas. *Stellar Atmospheres*. W. H. Freeman & Co., New York, 1978.

[16] R. S. Ronan, D. L. Mickey, and F. Q. Orrall. The Derivation of Vector Magnetic Fields from Stokes Profiles: Integral vs. Least Squares Fitting Techniques. *Sol. Phys.*, 113:353–359, 1987.

[17] Robert J. Rutten. Compendium solar spectrum formation. *arXiv e-prints*, art. arXiv:2103.02369, March 2021. URL `https://robrutten.nl/rrweb/rjr-pubs/2021LingAstRep...2R.pdf`.

[18] P. H. Scherrer, R. S. Bogart, R. I. Bush, J. T. Hoeksema, A. G. Kosovichev, J. Schou, W. Rosenberg, L. Springer, T. D. Tarbell, A. Title, C. J. Wolfson, I. Zayer, and MDI Engineering Team. The Solar Oscillations Investigation - Michelson Doppler Imager. *Sol. Phys.*, 162:129–188, December 1995. doi: 10.1007/BF00733429.

[19] J. Schou, P. H. Scherrer, R. I. Bush, R. Wachter, S. Couvidat, M. C. Rabello-Soares, R. S. Bogart, J. T. Hoeksema, Y. Liu, T. L. Duvall, D. J. Akin, B. A. Allard, J. W. Miles, R. Rairden, R. A. Shine, T. D. Tarbell, A. M. Title, C. J. Wolfson, D. F. Elmore, A. A. Norton, and S. Tomczyk. Design and Ground Calibration of the Helioseismic and Magnetic Imager (HMI) Instrument on the Solar Dynamics Observatory (SDO). *Sol. Phys.*, 275:229–259, January 2012. doi: 10.1007/s11207-011-9842-2.

[20] H. Socas Navarro, J. Trujillo Bueno, and B. Ruiz Cobo. Non-LTE Inversion of Stokes Profiles Induced by the Zeeman Effect. *ApJ*, 530:977–993, 2000.

[21] J. O. Stenflo. *Solar Magnetic Fields*. Kluwer Academic Publishers, 1994.